Available online at www.sciencedirect.com
ScienceDirect
International Journal of Heat and Fluid Flow 28 (2007) 1157–1166
International Journal of HEAT AND FLUID FLOW
www.elsevier.com/locate/ijhff

Macroscopic modeling of turbulent flow over a porous medium

H.C. Chan *, W.C. Huang, J.M. Leu, C.J. Lai

Department of Hydraulic and Ocean Engineering, Cheng-Kung University, Tainan 70101, Taiwan

Received 5 April 2005; received in revised form 19 September 2006; accepted 26 October 2006
Available online 17 January 2007

Abstract

Turbulent flow over a porous medium has been one of the most critical subjects in numerous environmental and engineering studies. The characteristics associated with the hybrid domain, involving both a porous region and a clear fluid region, are not fully understood primarily due to a lack of proper mathematical treatments of different regions and the fluid/porous interface. The objective of this study is to present a numerical implementation for examining such a hybrid domain. The governing equations were solved by a control volume method and the k–ε turbulent model in an attempt to predict the turbulent stresses. The present model treated the hybrid domain problem with a single domain approach by adopting the classical continuity interface conditions. Our numerical results were compared with the experimental data available in the literature for two cases. The effects of the porous medium on the flow properties, including porosity and permeability, were further investigated. Moreover, the calculated flow features were examined for three different Reynolds numbers. Results indicated that the penetration extent of turbulence was Darcy number- and porosity-dependent.

Keywords: Low-Reynolds number turbulent open channel flow; Porous medium; RANS modeling

1. Introduction

Transfer phenomena at the fluid/porous interface has remained an important topic of research because of its wide field of application in estimating the fluxes associated with dissolved organic molecules, inorganic ions, and fluid/gas flux between a porous surface and the overlying fluid (Nakamura and Stefan, 1994; Steinberger and Hondzo, 1999; Trussell and Chang, 1999; Jue, 2000; Vollmera et al., 2002; Miglio et al., 2003). Flows over a porous medium are characterized by a hybrid clear fluid-porous medium domain that flows both over and through the porous medium. The internal flow field of the porous medium remains coupled with the overlying fluid. The complex interaction between the overlying fluid and the internal fluid means the no-slip surface boundary condition is no longer applicable. In this fluid/porous interface problem, the flow interaction above and inside the porous medium, and the transfer mechanisms across the interface, deserve in-depth investigation.

The work of Beavers and Joseph (1967) is among the forerunners of research on the characteristics of fluid flow near the interface region. They found that the empirical relationship associated with the velocity across the interface could be discontinuous, which is described as a fluid slip phenomenon. However, several groups of researchers questioned the validity of this "slip velocity" and proposed the continuity of both the velocity and the shear stress at the interface (Neale and Nader, 1974; Vafai and Thiyagaraja, 1987; Vafai and Kim, 1989). In these investigations, the flow in the porous region was modeled using a semi-empirical Brinkman–Forchheimer's extended Darcy equation. The Brinkman term in this equation, representing the viscous effects, allows a no-slip boundary condition to be imposed at the impermeable wall and the matching of the momentum equations at the fluid/porous interface. Recently, Ochoa-Tapia and Whitaker (1995a), Ochoa-Tapia and Whitaker (1995b) utilized macroscopic variables

* Corresponding author. Tel.: +886 6 2757575x63268; fax: +886 6 2741463.
E-mail address: hcchan@mail.ncku.edu.tw (H.C. Chan).

0142-727X/$ - see front matter © 2006 Elsevier Inc. All rights reserved.
doi:10.1016/j.ijheatfluidflow.2006.10.005

Nomenclature

c_F	Forchheimer coefficient	P	pressure
c_k	dimensionless constant	P_k	production rate of k
$c_{\varepsilon 1}$, $c_{\varepsilon 2}$	k–ε turbulence model coefficients	R_f	Reynolds number
c_μ	coefficient for definition of v_t	R_T	turbulent Reynolds number
D	diameter of rod or glass bread	U, V	streamwise and vertical velocity components
Da	Darcy number $= K/H^2$	U_f	mean flow velocity
f_μ	damping function for v_t	U_*	friction velocity
f_1, f_2	damping functions for ε-equation	U^+	wall coordinates $= U/U_*$
G_k	extra generation rate of k	$-\overline{u_i u_j}$	Reynolds stress tensor
G_ε	extra production rate of ε	x, y	streamwise and vertical directions
H	channel depth	Y^+	wall coordinates $= yU_*/v$
h_f	clear fluid depth	δ_{ij}	Kronecher delta
h_p	porous depth	ε	dissipation rate of k
h_p^-	fluid located under the interface	κ	von Kármán constant
h_p^+	fluid located above the interface	v_t	turbulent (eddy) kinematic viscosity
K	permeability	v	fluid's kinematic viscosity
k	turbulent kinetic energy	σ_k, σ_ε	turbulent Prandtl numbers and
k^+	normalized turbulent kinetic energy $= k/U_*^2$	ϕ	porosity

and transport equations to study the flow in a porous medium and obtained the volume-averaged fluid properties. They also imposed the interface shear stress jump condition between the clear flow region and the porous medium for flow over a macroscopic interface area. However, the imposition of this interface condition is realized only by the use of an empirically determined constant. Silva and de Lemos (2003a), Silva and de Lemos (2003b) applied this shear stress jump condition to both laminar and turbulent flow over the porous medium. They have shown small changes in the empirical constant cause large variations in the curvature of the profile at the fluid/porous interface, which also provides some insight into the complexities of the interface region. In an effort to validate the matching boundary condition at the fluid/porous interface, Choi and Waller (1997) showed that the application of a single-domain approach could handle complex convection problems at the interface.

Notably, most of the studies cited deal with the low-Reynolds number flows. However, much remains unknown about the physical mechanisms associated with the turbulent flow over a porous medium. Moreover, turbulence in a porous medium is a controversial issue. With very small permeability and fluid velocity, the flow is often dominated by the laminar flow regime. Nevertheless, recent engineering applications have been developed from the interaction between turbulent flow and the porous medium. High-speed flow over or through such a highly permeable medium can lead to turbulent flow therein. Some investigations have elucidated the effect of turbulent flow above and through the porous medium (Zippe and Graf, 1983; Venkataraman and Rama Mohan Rao, 1998; Prinos et al., 2003). Mendoza and Zhou (1992) and Zhou and Mendoza (1993) presented analytical results concerning the turbulent flow characteristics and the velocity distribution in the clear fluid region, but did not investigate in detail the transport phenomena near the boundary of the permeable interface. Shimizu et al. (1990) conducted some experiments and provided a mathematical model to describe the velocities within the porous medium under turbulent flow. However, their model is based on a function of the slip velocity at the interface, which is not known a priori. Hence, applying such a mathematical model is rather difficult.

The numerical investigation of the turbulent flow within the porous region can use either a microscopic or macroscopic model. Using the microscopic model provides more detailed insight into the flow structure, but only solves the problems involving the porous media with simple geometrical characteristics. Prinos et al. (2003) presented microscopic computation of flow over and within a porous bed. They also provided very valuable measured data. Meanwhile, an efficient macroscopic model is required in order to investigate the turbulent flow within the porous medium with complex geometrical characteristics. Subsequent works on porous medium flow involve macroscopic turbulent models applied within a porous medium (e.g., Wang and Takle, 1995; Antohe and Lage, 1997; Travkin and Catton, 1995; Kuwahara et al., 1998; Nakayama and Kuwahara, 1999; Masuoka and Takatsu, 1996; Takatsu and Masuoka, 1998; Getachew et al., 2000; Pedras and de Lemos, 2000, 2001a,b). A synthesis of the turbulent models that have been applied within the porous medium can also be found in Vafai et al. (2005). The macroscopic turbulent model describes the characteristics of fluid flow within a porous medium by the volume-averaged variables. The additional terms required for fluid–particle interactions are incorporated in the momentum equations and turbulent models. The macroscopic turbulent model as

derived by Pedras and de Lemos (2000) has a better characterization of the flow turbulent kinetic energy. This model is a k–ε model based on the formulations developed from the numerical results, including the use of spatially periodic circular and elliptic rods to represent porous matrixes. The model is, however, yet to be validated against a range of porous media.

In the present study, the characteristics of turbulent flow in a channel partially filled with a fluid-saturated homogeneous porous medium are studied numerically. The turbulent flow in the clear fluid region is described by the RANS equations, while the flow in the porous region is described by the extended Darcy equation together with the macroscopic turbulent model of Pedras and de Lemos (2001a), Pedras and de Lemos (2001b). The present model was successfully used to simulate the turbulent flow over a porous medium as demonstrated by the previous studies of Shimizu et al. (1990) and Prinos et al. (2003). In order to further contribute to our understanding of the fundamental characteristics of turbulence over and within the porous medium, the dependence of the porous properties on numerous parameters of the problem are extensively investigated and discussed. The effects of the Reynolds number R_f (based on the mean flow velocity U_f and on the clear fluid depth h_f), the dimensionless permeability, which is given by Darcy number Da ($=K/H^2$, $K=$ permeability and $H=$ channel depth), and the porosity ϕ are emphasized in this study.

2. Mathematical formulations

Fig. 1 schematically depicts the coordinate system and the corresponding physical configuration. The two-dimensional, incompressible, isothermal, and steady flow is assumed to be inside a rectangular channel partially filled with a layer of homogeneous porous medium. At the bottom is an impermeable wall. Additionally, the physical properties of the fluid and the porous medium are assumed to be constant. Flow in the porous medium may be distinguished into two sub-regions: (a) the interface boundary layer region located in the upper part of the porous medium and characterized by rapid changes between the slip velocity and the Darcy velocity; and (b) the uniform Darcy velocity region.

2.1. Governing equations in the clear fluid region

The turbulent flow in the clear fluid region can be described by the RANS equations. The steady-state forms of the continuity and momentum equations are written as

$$\frac{\partial U_i}{\partial x_i}=0 \tag{1}$$

$$U_j\frac{\partial U_i}{\partial x_j}=-\frac{1}{\rho}\frac{\partial P}{\partial x_i}+\frac{\partial}{\partial x_j}\left[\nu\left(\frac{\partial U_i}{\partial x_j}+\frac{\partial U_j}{\partial x_i}\right)-\overline{u_iu_j}\right] \tag{2}$$

where U_i is the velocity in the x_i direction; P is the fluid pressure; $-\overline{u_iu_j}$ are the Reynolds stresses; ρ is the density of the fluid; and ν is the fluid's kinematic viscosity. The eddy viscosity concept is used to specify the unknown $-\overline{u_iu_j}$,

$$-\overline{u_iu_j}=\nu_t\left(\frac{\partial U_i}{\partial x_j}+\frac{\partial U_j}{\partial x_i}\right)-\frac{2}{3}\delta_{ij}k \tag{3}$$

where ν_t is the eddy viscosity; δ_{ij} is the Kronecher delta; and $k\left(=\frac{1}{2}\overline{u_i^2}\right)$ is the turbulent kinetic energy. The eddy viscosity ν_t is a function of k and its rate of dissipation ε as

$$\nu_t=f_\mu c_\mu\frac{k^2}{\varepsilon} \tag{4}$$

where c_μ is an empirical constant, and f_μ is the damping function. Subsequently, transport equations are required for k and ε to close the problem. The following transport equations for k and ε are solved:

$$U_j\frac{\partial k}{\partial x_j}=P_k+\frac{\partial}{\partial x_j}\left[\left(\nu+\frac{\nu_t}{\sigma_k}\right)\frac{\partial k}{\partial x_j}\right]-\varepsilon \tag{5}$$

$$U_j\frac{\partial \varepsilon}{\partial x_j}=c_{\varepsilon1}f_1\frac{\varepsilon}{k}P_k+\frac{\partial}{\partial x_j}\left[\left(\nu+\frac{\nu_t}{\sigma_\varepsilon}\right)\frac{\partial \varepsilon}{\partial x_j}\right]+c_{\varepsilon2}f_2\frac{\varepsilon^2}{k} \tag{6}$$

where $P_k\left(=-\overline{u_iu_j}\frac{\partial U_i}{\partial x_j}\right)$ is the production rate of k determined by the gradients of U_i; f_1 and f_2 are the damping functions; and $c_{\varepsilon1}$, $c_{\varepsilon2}$, σ_k and σ_ε are dimensionless constants. Launder and Sharma's (1974) low-Reynolds model

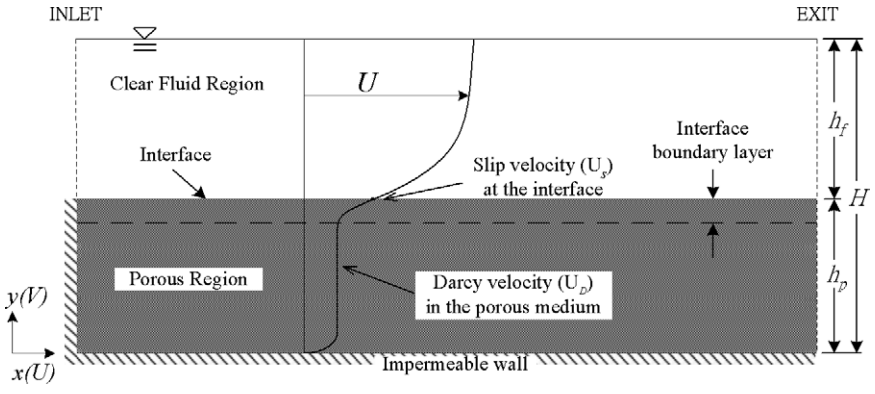

Fig. 1. Coordinate system and the schematic physical configuration.

is employed here, and the following damping functions are applied:

$$f_\mu = \exp\left[\frac{-3.4}{(1+R_T/50)^2}\right] \tag{7}$$

$$f_1 = 1 \tag{8}$$

$$f_2 = 1 - 0.3\exp(-R_T^2) \tag{9}$$

where $R_T(=k^2/v\varepsilon)$ is the turbulent Reynolds number. The use of this low-Reynolds model is justified in regions (near the interface) where Reynolds numbers are relatively low. The interaction of the turbulent flow and porous medium may result in the penetration of flow into the porous medium and the traditional wall function fails near the interface region. The present calculations are performed with many refined grid points near the interface and without using the wall function for the first grid above the interface.

2.2. Governing equations in the porous region

Depending on the perspective, "macroscopic" or "microscopic" equations can be applied to the porous medium. Most flow properties considered in practical engineering situations are macroscopic manifestations of flow inside a representative elementary volume (REV), so the Forchheimer's extended Darcy equation is used in this study to describe the flow properties within the pores on a macroscopic level. The macroscopic continuity and momentum equations are expressed as:

$$\frac{\partial U_i}{\partial x_i} = 0 \tag{10}$$

$$U_j\frac{\partial U_i}{\partial x_j} = -\frac{1}{\rho}\frac{\partial P}{\partial x_i} + \frac{\partial}{\partial x_j}\left[v\left(\frac{\partial U_i}{\partial x_j}+\frac{\partial U_j}{\partial x_i}\right) - \overline{u_i u_j}\right] - \phi\frac{v}{K}U_i - \phi^2\frac{c_F}{\sqrt{K}}\sqrt{U_jU_j}U_i \tag{11}$$

where ϕ represents the porosity; K is the permeability; and c_F is the Forchheimer coefficient. The last two terms in Eq. (11) represent the drag force due to the presence of the porous medium. The generalized model Eq. (11) reduces to the RANS equations when the porous matrix disappears, as $\phi \to 1$ and $K \to \infty$. The macroscopic k–ε turbulent model of Pedras and de Lemos (2001a), Pedras and de Lemos (2001b), as obtained by applying the volume-averaging operator to the microscopic k–ε equations inside a REV, is used herein. It is given by:

$$U_j\frac{\partial k}{\partial x_j} = P_k + \frac{\partial}{\partial x_j}\left[\left(v+\frac{v_t}{\sigma_k}\right)\frac{\partial k}{\partial x_j}\right] + G_k - \varepsilon \tag{12}$$

$$U_j\frac{\partial \varepsilon}{\partial x_j} = c_{\varepsilon 1}f_1\frac{\varepsilon}{k}P_k + \frac{\partial}{\partial x_j}\left[\left(v+\frac{v_t}{\sigma_\varepsilon}\right)\frac{\partial \varepsilon}{\partial x_j}\right] + c_{\varepsilon 2}\left(G_\varepsilon - f_2\frac{\varepsilon^2}{k}\right) \tag{13}$$

where $G_k\left(=c_k\phi\frac{k}{\sqrt{K}}\sqrt{U_jU_j}\right)$ is the extra generation rate of k due to the presence of the porous medium; $G_\varepsilon\left(=c_k\phi\frac{\varepsilon}{\sqrt{K}}\sqrt{U_jU_j}\right)$ is the extra production rate of ε due to the presence of the porous medium; and c_k is a dimensionless constant. These extra terms (G_k and G_ε) vanish in the limiting case in which no porous medium is present, or the porosity and the permeability are extremely high ($\phi \to 1$ and $K \to \infty$), meaning that the transport equations of k and ε are recovered to the clear fluid region.

3. Numerical simulation

The suitable boundary conditions of Fig. 1 on the inlet, outlet, the impermeable wall and the top are straightforward in this study. The uniform flow enters through the channel inlet; the fully developed convective exit condition is specified at the exit; the no-slip condition is applied to the impermeable wall and the symmetry condition is imposed at the top of the channel. Suitable interface conditions for mass, momentum and the transport equations for k and ε at the interface are, however, still not well established. While controversies remain regarding these conditions at the microscopic/macroscopic level (Ochoa-Tapia and Whitaker, 1995a,b; Kuznetsov, 1997; Alazmi and Vafai, 2001), in this work, for simplicity, the classical continuity boundary conditions are applied at the interface. The following interface conditions, therefore, need to be satisfied:

$$U_i|_{y=h_p^-} = U_{iy=h_p^+} \tag{14}$$

$$P|_{y=h_p^-} = P|_{y=h_p^+} \tag{15}$$

$$v\left(\frac{\partial U_i}{\partial x_j}+\frac{\partial U_j}{\partial x_i}\right)\Big|_{y=h_p^-} = v\left(\frac{\partial U_i}{\partial x_j}+\frac{\partial U_j}{\partial x_i}\right)\Big|_{y=h_p^+} \tag{16}$$

$$k|_{y=h_p^-} = k|_{y=h_p^+} \tag{17}$$

$$\left(v+\frac{v_t}{\sigma_k}\right)\frac{\partial k}{\partial x_j}\Big|_{y=h_p^-} = \left(v+\frac{v_t}{\sigma_k}\right)\frac{\partial k}{\partial x_j}_{y=h_p^+} \quad \varepsilon|_{y=h_p^-} = \varepsilon|_{y=h_p^+} \tag{18}$$

$$\left(v+\frac{v_t}{\sigma_\varepsilon}\right)\frac{\partial \varepsilon}{\partial x_j}\Big|_{y=h_p^-} = \left(v+\frac{v_t}{\sigma_\varepsilon}\right)\frac{\partial \varepsilon}{\partial x_j}\Big|_{y=h_p^+} \tag{19}$$

where subscripts h_p^- and h_p^+ refer to the fluid located under and above the interface, respectively. Interface conditions (14) to (16) express the continuity of velocity, pressure and shear stress, respectively. Choi and Waller (1997) developed the interface conditions (14)–(16) used in the laminar regime. In the present study, we extend the functions developed for the turbulent regime. The interface conditions (17)–(20) specify the continuity of k, ε and their fluxes across the interface, which were previously used by Lee and Howell (1987) and de Lemos and Pedras (2000). A more detailed discussion of interface conditions (18) is found in de lemos (2005).

As mentioned earlier, Eqs. (11)–(13) reduce to the clear fluid condition as the porous matrix disappears ($\phi \to 1$ and $K \to \infty$). Therefore, the single-domain approach, proposed by Choi and Waller (1997), can be used to solve fluid/porous interface problems by appropriately changing the properties of the porous medium in the computational

domain. For the present calculations, the following porosity and permeability limits are applied for the porous region and clear fluid region:

$$\begin{matrix}\phi = 1 \\ K \to \infty\end{matrix} \Rightarrow \text{clear fluid region} \quad \begin{matrix}\phi < 1 \\ K = finite\end{matrix} \Rightarrow \text{porous region} \tag{20}$$

Notably, this approach has been thoroughly tested and validated by Vafai and Kim (1990) and Choi and Kim (1994). It has been shown that the numerical solutions automatically satisfy the continuity of velocities, shear stresses and fluxes across the fluid/porous interface without an additional iterative procedure to match the interface conditions as described in Eqs. (14)–(20).

A control-volume method of Patankar (1980), based on an orthogonal Cartesian coordinate system, is applied to discretize the continuity, momentum and turbulent model equations with the SIMPLE algorithm. Non-staggered grids are used depending on the aspect ratio of the calculation domain. Furthermore, very dense grids are located around the fluid/porous interface.

4. Model tests

The macroscopic equations discussed above yield the averaged characteristics of the modeled flow in a fluid-saturated porous medium. The best way to increase insight into the understanding of the macroscopic model is to compare it with the microscopic and experimental data. Accordingly, the computational conditions, including boundary conditions, clear fluid/porous regions and position of interface presented in this paper were set to match the conditions of the available reference data.

Case 1: Flow in a channel partially filled with a bundle of rods

Prinos et al. (2003) numerically and experimentally investigated fully developed and uniform flow in a flume with a porous bed, as presented in Fig. 2a. The flume was 12 m long, 0.25 m wide and 0.5 m high. The porous bed was simulated using spatially periodic rods with a diameter D of 1.0 cm in a non-staggered pattern. The porous depth h_p was kept constant and equal to 5.5 cm, the porosity ϕ was 0.8286, and the permeability K was 4.017×10^{-4} m^2. Table 1 displays the geometric and hydrodynamic characteristics of the flow. In the experimental cases A and B (Table 1), the clear fluid depth h_f were 3 cm and 5 cm, and the Reynolds numbers R_f were 7581 and 10,780, respectively.The computational domain consists of 81×91 nodes. Fig. 3 plots the turbulent velocities above the fluid/porous interface in both the cases, as obtained by using the present model. The velocities are presented in wall coordinates $Y^+(=yU_*/v)$ and $U^+(=U/U_*)$ to enable them to be directly compared with both the measured and microscopic data by Prinos et al. (2003). The linear velocity distribution in the viscous inner region, $Y^+ = U^+$, and the logarithmic law in the outer (fully turbulent) region, $U^+ = (1/\kappa)\ \ln(Y^+) + B(\kappa = 0.41,\ \ B = 5.25)$, for flow over a smooth impermeable wall are also plotted. The presence of the porous medium causes a significant reduction of the velocities in the clear fluid region, compared to the flow over the smooth impermeable wall. This is due to the penetration of the turbulence and

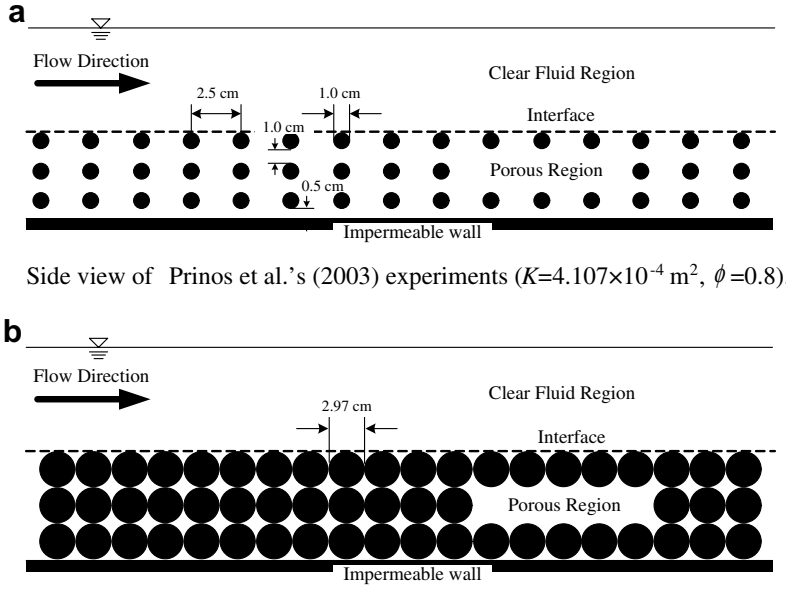

Fig. 2. Schematic diagram of the model tests.

Table 1
Measured experimental parameters from Prinos et al. (2003) and Shimizu et al. (1990)

Parameter	Description	$A1$	$A2$	$B1$	$B2$	$B3$
K	Permeability (m^2)	4.107×10^{-4}	4.107×10^{-4}	2.8×10^{-7}	2.8×10^{-7}	2.8×10^{-7}
Da	Darcy Number	5.684×10^{-2}	3.725×10^{-2}	1.317×10^{-5}	9.122×10^{-6}	8.827×10^{-6}
ϕ	Porosity	0.8286	0.8286	0.38	0.38	0.38
H	Total depth (mm)	85	105	145.8	175.2	178.1
h_f	Free flow depth (mm)	30	50	56.7	86.1	59.1
h_f/H	Relative depth	0.3529	0.4762	0.3889	0.4914	0.3318
R_f	Reynolds number	7.581×10^{3}	1.437×10^{4}	2.351×10^{4}	3.869×10^{4}	2.339×10^{4}

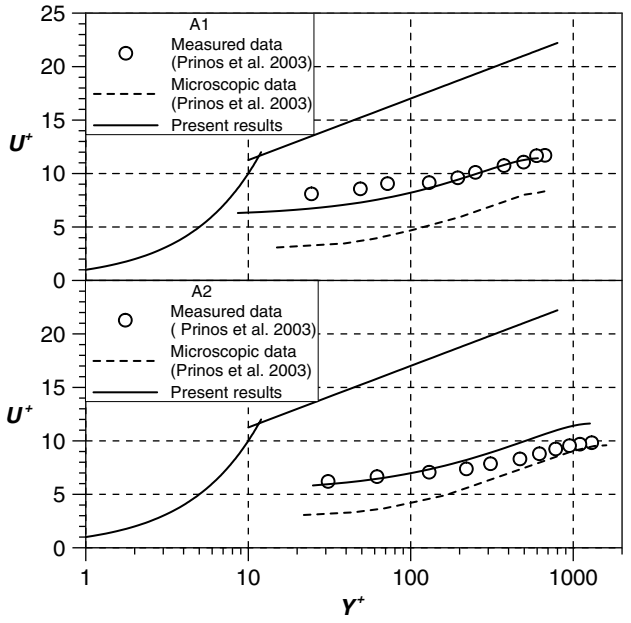

Fig. 3. Measured (Prinos et al., 2003) vs. computed velocity distribution above porous medium. Lines, computations; symbols, measurements.

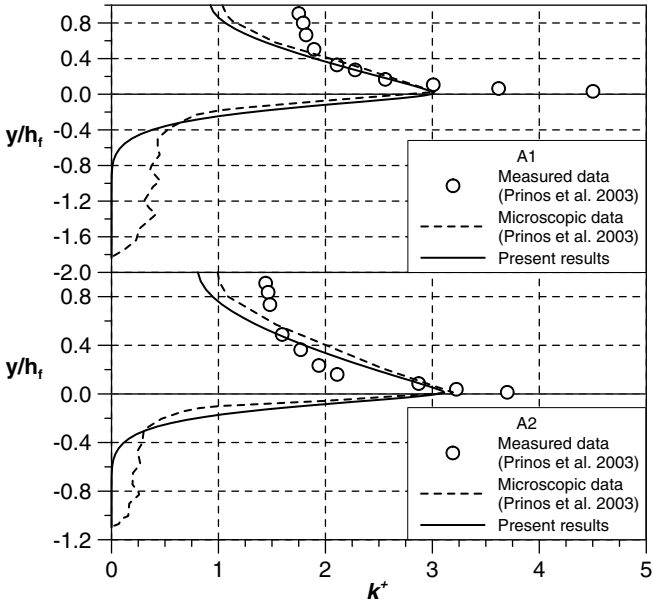

Fig. 4. Measured (Prinos et al., 2003) vs. computed turbulent kinetic energy over the whole depth. Lines, computations; symbols, measurements.

the momentum exchange near the fluid/porous interface. The present model indicates superior agreement with the measured data over the microscopic data. Fig. 4 shows the normalized turbulent kinetic energy $k^+(=k/U_*^2)$ for these two cases (A and B in Table 1), using the present model. Fig. 4 also shows the corresponding measured and microscopic data by Prinos et al. (2003). The present model and microscopic data are in satisfactory agreement both over and within the porous region. The penetration of turbulent kinetic energy into the porous region appears significant. Notably, within the porous region, the present model approximates the microscopic data in an average sense. On the other hand, the levels of measured data are higher than the present model in the clear fluid region. This is because Prinos et al. (2003) estimated the turbulent kinetic energy from three normal stresses. However, a general trend can be found from the present model which indicates the maximum values of k^+ occur extremely close to the interface.

Case 2: Flow in a channel partially filled with glass beads

Shimizu et al. (1990) performed experiments in a laboratory flume, as shown in Fig. 2b, which was 8 m long, 0.21 m wide. The flume was partially filled with glass beads (with diameter, $D = 2.97$ cm) that were arranged in the most tightly packed tetragonal-spheroidal pattern as a model of the porous medium. Table 1 also presents the experimental conditions performed by Shimizu et al. (1990). The porous medium had a porosity ϕ of 0.38 and the permeability K of 2.8×10^{-7} m^2. In the experimental cases (B1, B2 and B3 in Table 1), the clear fluid depth h_f was 5.67 cm, 8.61 cm and 5.91 cm, respectively, for the porous depths h_p of 8.91 cm, 8.91 cm and 11.9 cm and the Reynolds numbers R_f equal to 23,510, 38,690 and 23,390. The velocity measurements within the porous medium were estimated from the time difference between the peak concentrations recorded at two density-meters (for salt water) at the same height.

In all experimental runs herein, the present model together with 81×91 computational nodes was also successful. Fig. 5 compares the computed velocity distributions U/U_f below the fluid/porous interface with the experimental data obtained by Shimizu et al. (1990). Notably, the present numerical model accurately represents the general

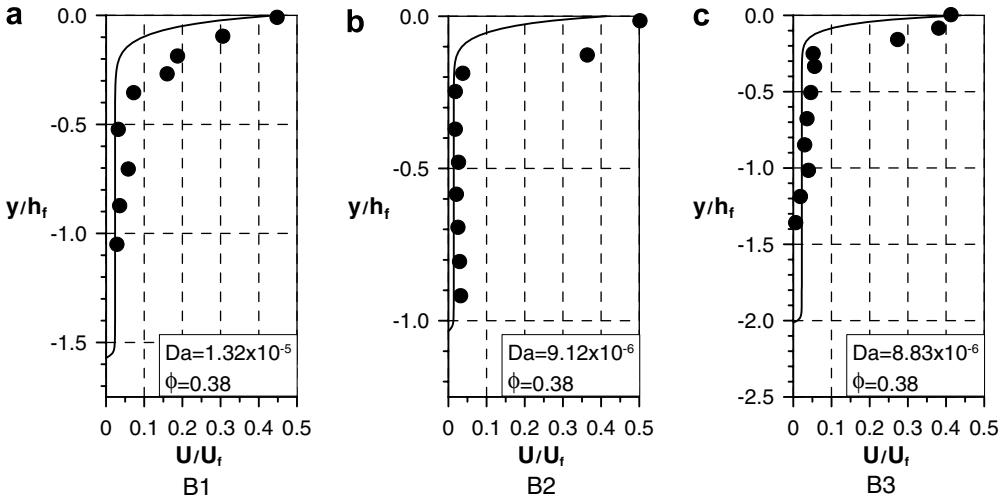

Fig. 5. Measured (Shimizu et al., 1990) vs. computed velocity distribution within porous medium. Lines, computations; symbols, measurements.

trend of the velocity distributions. The interface velocities are quite high, with values varying from 0.41 to 0.5, which are much higher than the respective laminar flow values over a porous medium, as predicted by Choi and Waller (1997). Importantly, the computed velocity distributions agree with the experimental data at the fluid/porous interface and Darcy velocity region, but a slight difference is evident in the interface boundary layer region. As pointed by Dancey et al. (2000), this be explained by the fact that both the vertical mean velocities and the vertical momentum fluxes demonstrate strong inhomogeneity of the turbulence pattern in the interface area. For a 2-D fully developed flow, the conservation of mass would require $V = 0$, where the effects of vertical fluid motion between the gaps among the glass breads are not taken into account.

5. Results and analyses

This paper, consider steady flow inside a rectangular channel that is partly filled with the porous medium, through which fluid flows in the turbulent regime. The experimental configurations of Prinos et al. (2003) and Shimizu et al. (1990) are used as the basis for determining the parameters in the sensitivity analysis as presented in this study. Table 2 summarizes the parameters selected from the range of these experiments. Fig. 6 presents the variation of the computed velocity profiles, normalized with U_f, for the three values of R_f (R_f varying from 9444 to 11,820) at the same Darcy number $Da(=2.5\times10^{-3})$ and $\phi(=0.6)$. The turbulent flow propagates across the interface into the porous medium and forms an interface boundary layer region in the upper part of the porous medium. Note that in absence of the slip boundary condition no boundary layer will be formed in the porous medium. This indicates that Darcy's law alone is unable to fully describe flow in a porous medium. Evidently, the difference in Reynolds numbers does not cause the velocity profiles through the clear passage and the porous medium to differ. Fig. 7 presents the corresponding distribution of the normalized turbulent kinetic energy $k^+(=k/U_*^2)$ above and within the porous region. The penetration of k^+ into the porous area is visible in the upper part of the porous medium. The turbulent kinetic energy peaks form close to the fluid/porous interface and then decreases continuously as the free surface and impermeable wall are approached. Within the range of analyzed R_f, the penetration of the turbulence, however, remains independent of the Reynolds number.

Fig. 8 shows the normalized velocity profiles of the fully developed flow for Da varying from 2.5×10^{-5} to 2.5×10^{-3} and with a fixed porosity $\phi = 0.6$. The velocity profiles in Fig. 8 demonstrate that a greater Da value (higher permeability) corresponds to more flow through

Table 2
Parameters used in the sensitivity analysis

Parameter	Description	Run1	Run2	Run3	Run4	Run5	Run6	Run7
K	Permeability (m^2)	1.0×10^{-4}	1.0×10^{-4}	1.0×10^{-4}	1.0×10^{-4}	1.0×10^{-5}	1.0×10^{-6}	1.0×10^{-4}
Da	Darcy number	2.5×10^{-3}	2.5×10^{-3}	2.5×10^{-3}	2.5×10^{-3}	2.5×10^{-4}	2.5×10^{-5}	2.5×10^{-3}
ϕ	Porosity	0.6	0.6	0.6	0.8	0.8	0.8	0.7
H	Total depth (mm)	200	200	200	200	200	200	200
h_f	Free flow depth (mm)	100	100	100	100	100	100	100
h_f/H	Relative depth	0.5	0.5	0.5	0.5	0.5	0.5	0.5
R_f	Reynolds number	9.444×10^3	1.063×10^4	1.182×10^4	1.170×10^4	1.195×10^4	9.671×10^3	1.178×10^4

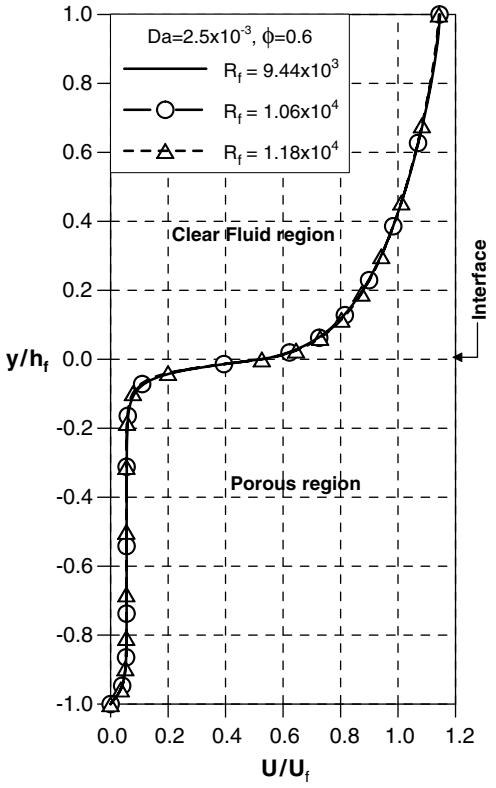

Fig. 6. Velocity distribution above and within the porous region for different Reynolds number R_f.

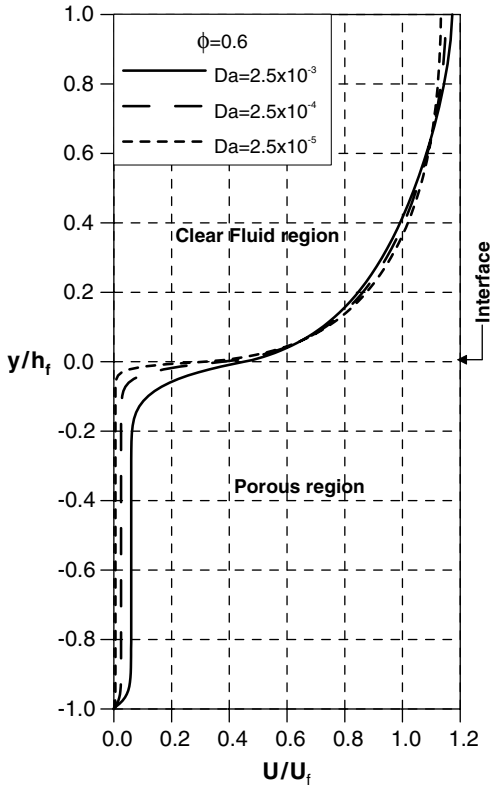

Fig. 8. Effect of Darcy number Da on velocity distribution above and within the porous region.

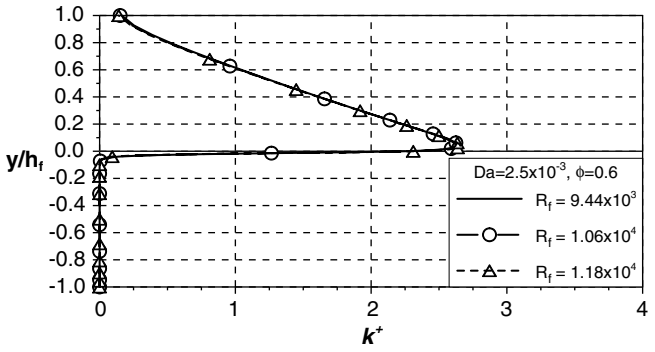

Fig. 7. Turbulent kinetic energy above and within the porous region for different Reynolds number R_f.

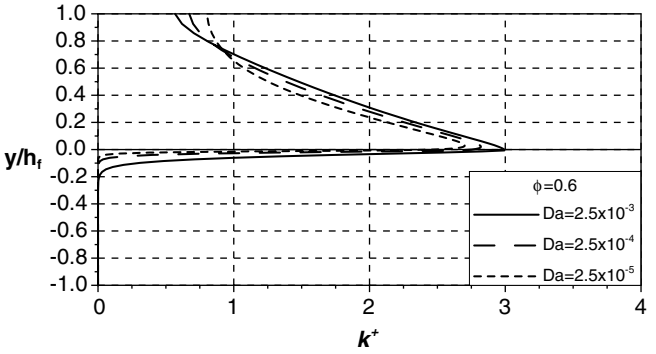

Fig. 9. Effect of Darcy number Da on turbulent kinetic energy above and within the porous region.

the porous substance in the region $0 < y/h_f < -1.0$. Moreover, the interface velocity gradient increases rapidly as Da decreases. This increase in velocity gradient is caused by the damping effect of the porous material and approaches the flow over an impermeable bed, because neither penetration of fluid nor the damping force exists in the porous region. In Fig. 9, the normalized turbulent kinetic energy k^+ above and within the porous region are plotted to exhibit the effect of Da. The penetration of the turbulent kinetic energy into the porous region also remains considerable. Significant levels of k^+ increase with Da in the porous region. For the case with the highest Da value ($Da = 2.5 \times 10^{-3}$), the penetration of k^+ extends to $y/h_f = -0.2$. It is shown that the extra generation term in the k-equation becomes more important in determining the level of turbulent kinetic energy in highly permeable materials.

Fig. 10 presents the effect of porosity ϕ on the normalized velocity profiles. As expected, the greater porosity causes a higher flow through the porous medium. Similar trends are observed in Fig. 11, as the corresponding curves of the normalized turbulent kinetic energy in the interface region slightly increase with ϕ. This fact is explained by the extra generation term in the k-equation, which is proportional to velocities within the porous medium. Interestingly, all the cases presented herein involve a fixed total

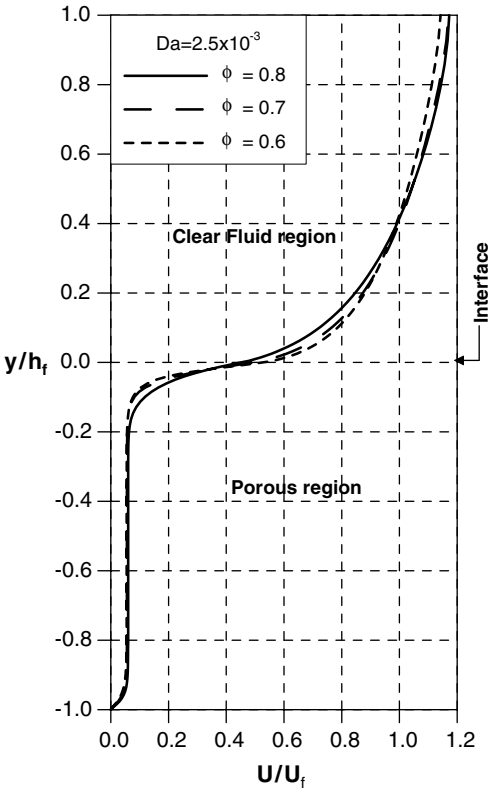

Fig. 10. Effect of porosity ϕ on velocity distribution above and within the porous region.

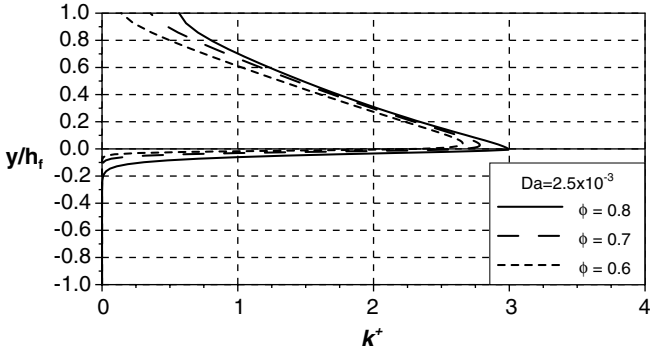

Fig. 11. Effect of porosity ϕ on turbulent kinetic energy above and within the porous region.

flow rate through the channel, but the flow characteristics within the porous medium depend significantly on the permeability of the medium.

6. Conclusions

The work presents the numerical solutions for turbulent 2-D flow in a channel with a porous medium. At the fluid/porous interface the flow is continuous, so the single-domain approach is applied in the numerical implementation when dealing with such a hybrid domain. A comparison with existing experimental data strictly validates the numerical tool developed for situations where the Reynolds number, the Darcy number and the porosity are varied. Increase in the Darcy number and the porosity enhance the penetration of turbulence. The slip velocity at the interface plays a particularly important role for turbulent flow over the porous medium. The distributions of turbulent kinetic energy demonstrate that, in the simulated case of high permeability, the existence of an extra production term in the k-equation is important in the porous region. Higher Darcy number values significantly increase the penetration of turbulence into the upper part of the porous medium. These findings on the behavior of turbulent flow over a porous medium clearly indicate that the level of turbulent penetration depends strongly on the damping effect of the porous medium itself.

Acknowledgements

The authors thank the National Science Council of the Republic of China for financially supporting this research under Contract No. NSC 92-2211-E-006-031. The first author wishes to thank the members of National Center for Computational Hydroscience and Engineering (NCCHE, The University of Mississippi) for their helpful comments.

References

Alazmi, B., Vafai, K., 2001. Analysis of fluid flow and heat transfer interfacial conditions between a porous medium and fluid layer. Int. J. Heat Mass Transfer 44, 1735–1749.

Antohe, B.V., Lage, J.L., 1997. A general two-equation macroscopic turbulence model for incompressible flow in porous media. Int. J. Heat Mass Transfer 40, 3013–3024.

Beavers, G.S., Joseph, D.D., 1967. Boundary conditions at a naturally permeable wall. J. Fluid Mech. 30, 197–207.

Choi, C.Y., Kim, S.J., 1994. Modeling of boundary conditions at the soil and water interface. In: Proceedings of the ASAE International Winter Meeting. Am. Soc. Agric. Engrs. St. Joseph. Mich.

Choi, C.Y., Waller, P.M., 1997. Momentum transport mechanism for water flow over porous media. J. Environ. Engrg. 123 (8), 792–799.

Dancey, C.L., Balakrishnan, M., Diplas, P., Papanicolaou, A.N., 2000. The spatial inhomogeneity of turbulence above a fully rough, packed bed in open channel flow. Exp. Fluids 29 (5), 402–410.

de lemos, M.J.S., 2005. Turbulent kinetic energy distribution across the interface between a porous medium and a clear region. Int. Commun. Heat Mass Transfer 32 (1–2), 107–115.

de Lemos, M.J.S., Pedras, M.H.J., 2000. Simulation of turbulent flow through hybrid porous medium-clear fluid domains. Proc. ASME Heat Transfer Div. 5, 113–122.

Getachew, D., Minkowycz, W.J., Lage, J.L., 2000. A modified form of the k–ε model for turbulent flow of an incompressible fluid in porous media. Int. J. Heat Mass Transfer 43, 2909–2915.

Jue, C.T., 2000. Analysis of oscillatory flow with thermal convection in a rectangular cavity filled with porous medium. Int. Commun. Heat Mass Transfer 27 (7), 985–994.

Kuwahara, F., Kameyama, Y., Yamashita, S., Nakayama, A., 1998. Numerical modeling of turbulent flow in porous media using a spatially periodic array. J. Porous Media 1, 47–55.

Kuznetsov, A.V., 1997. Influence of the stress jump condition at the porous-medium clear-fluid interface on a flow at a porous wall. Int. Commun. Heat Mass Transfer 24 (3), 401–417.

Launder, B.E., Sharma, B.I., 1974. Application of the energy dissipation model of turbulence to the calculation of flow near a spinning disk. Lett. Heat Mass Transfer 3, 269–289.

Lee, K., Howell, J.R., 1987. Forced convective and radiative transfer within a highly porous layer exposed to a turbulent external flow field. Proc. ASME-JSME Therm. Engrg. Joint Conf. 2, 377–386.

Masuoka, T., Takatsu, Y., 1996. Turbulence model for flow through porous media. Int. J. Heat Mass Transfer 39, 2803–2809.

Mendoza, C., Zhou, D., 1992. Effect of porous bed on turbulent stream flow above bed. J. Hydraul. Engrg. 118 (9), 1222–1240.

Miglio, E., Quarteroni, A., Saleri, F., 2003. Coupling of free surface and groundwater flows. Comput. Fluids 32, 73–83.

Nakamura, Y., Stefan, H.G., 1994. Effect of flow velocity on sediment oxygen demand: theory. J. Hydraul. Engrg. 120 (5), 996–1016.

Nakayama, A., Kuwahara, F., 1999. A macroscopic turbulence model for flow in a porous medium. J. Fluids Engrg. 121, 427–433.

Neale, G., Nader, W., 1974. Practical significance of Brinkman's extension of Darcy's law: coupled parallel flows within a channel and a bounding porous medium. Can. J. Chem. Engrg 52, 475–478.

Ochoa-Tapia, J.A., Whitaker, S., 1995a. Momentum transfer at the boundary between a porous medium and a homogeneous fluid I: theoretical development. Int. J. Heat Mass Transfer 38, 2635–2646.

Ochoa-Tapia, J.A., Whitaker, S., 1995b. Momentum transfer at the boundary between a porous medium and a homogeneous fluid II: comparison with experiment. Int. J. Heat Mass Transfer 38, 2647–2655.

Patankar, S.V., 1980. Numerical Heat Transfer and Fluid Flow. Hemisphere, New York.

Pedras, M.H.J., de Lemos, M.J.S., 2000. On the definition of turbulent kinetic energy for flow in porous media. Int. Commun. Heat Mass Transfer 27 (2), 211–220.

Pedras, M.H.J., de Lemos, M.J.S., 2001a. Macroscopic turbulence modeling for incompressible flow through undeformable porous media. Int. J. Heat Mass Transfer 44 (6), 1081–1093.

Pedras, M.H.J., de Lemos, M.J.S., 2001b. Simulation of turbulent flow in porous media using a spatially periodic array and a low Re two-equation closure. Numer. Heat Transfer Part A 39 (1), 35–59.

Prinos, P., Sofialidis, D., Keramaris, E., 2003. Turbulent flow over and within a porous bed. J. Hydraul. Engrg. 129 (9), 720–733.

Shimizu, Y., Tsujimoto, T., Nakagawa, H., 1990. Experimental and macroscopic modeling of flow in highly porous medium under free-surface flow. J. Hydrosci. Hydraul. Engrg. 8 (1), 69–78.

Silva, R.A., de Lemos, M.J.S., 2003a. Numerical analysis of the stress jump interface condition for laminar flow over a porous layer. Numer. Heat Transfer Part A 43 (6), 603–617.

Silva, R.A., de Lemos, M.J.S., 2003b. Turbulent flow in a channel occupied by a porous layer considering the stress jump at the interface. Int. J. Heat Mass Transfer 46, 5113–5121.

Steinberger, N., Hondzo, M., 1999. Diffusional mass transfer at sediment–water interface. J. Environ. Engrg. 125 (2), 192–199.

Takatsu, Y., Masuoka, T., 1998. Turbulent phenomena in flow through porous media. J. Porous Media 3, 243–251.

Travkin, V.S., Catton, I., 1995. A two temperature model for turbulent flow and heat transfer in a porous layer. J. Fluids Engrg. 117, 181–188.

Trussell, R.R., Chang, M., 1999. Review of flow through porous media as applied to head loss in water filters. J. Env. Engrg. 125 (11), 998–1006.

Vafai, K., Kim, S.J., 1989. Forced convection in a channel filled with a porous medium: an exact solution. ASME J. Heat Transfer 111, 1103–1106.

Vafai, K., Kim, S.J., 1990. Analysis of surface enhancement by a porous substrate. ASME J. Heat Transfer 112, 700–706.

Vafai, K., Thiyagaraja, R., 1987. Analysis of flow and heat transfer at the interface region of a porous medium. Int. J. Heat Mass Transfer 30, 1391–1405.

Vafai, K., Khanafer, K., Minkowycz, W.J., Bejan, A., 2005. Synthesis of models for turbulent transport through porous media. Handbook of Numerical Heat Transfer. Wiley, New York.

Venkataraman, P., Rama Mohan Rao, P., 1998. Darcian, transitional, and turbulent flow through porous media. J. Hydraul. Engrg. 124 (8), 840–846.

Vollmera, S., Ramos, F.S., Daebel, H., Kühn, G., 2002. Micro scale exchange processes between surface and subsurface water. J. Hydrol. 269, 3–10.

Wang, H., Takle, E.S., 1995. Boundary-layer flow and turbulence near porous obstacles. Boundary-Lay. Meteorol. 74, 73–88.

Zhou, D., Mendoza, C., 1993. Flow through porous bed of turbulent stream. J. Engrg. Mech. 119 (2), 365–383.

Zippe, H.J., Graf, W.H., 1983. Turbulent boundary-layer flow over permeable and nonpermeable rough surfaces. J. Hydraul. Res. 21 (1), 51–65.